Supplementary Information

Tailored MXene-derived Nano-Heterostructure Oxide for Peroxymonosulfate Activation in the Treatment of Municipal Wastewaters

Shalu Atri,[a,b*], Elham Loni,[b] Zuzana Dyrcikova,[c] Frantisek Zazimal,[d] Maria Caplovicova,[e] Dana Dvoranova,[c] Gustav Plesch,[a] Miroslava Kabatova,[f] Marcello Brigante,[g] Michael Naguib,[b,h*] Olivier Monfort[a*]

[a] Department of Inorganic Chemistry, Faculty of Natural Sciences, Comenius University Bratislava, Ilkovicova 6, Mlynska Dolina, SK-842 15 Bratislava, Slovak Republic

[b] Department of Physics and Engineering Physics, Tulane University, New Orleans, Louisiana 70118, United States of America

[c] Institute of Physical Chemistry and Chemical Physics, Faculty of Chemical and Food Technology, Slovak University of Technology in Bratislava, Radlinskeho 9, SK-812 37 Bratislava, Slovak Republic

[d] Department of Plasma Physics and Technology, Faculty of Science, Masaryk University, Kotlarska 267/2, 611 37 Brno, CZ-602 00, Czech Republic

[e] STU Center for Nanodiagnostics, Faculty of Materials Science and Technology in Trnava, Slovak University of Technology in Bratislava, Vazovova 5, SK-812 43 Bratislava, Slovak Republic

[f] Bratislavská vodárenská spoločnosť a.s., Prešovská 48, 826 46 Bratislava, Slovak Republic

[g] Université Clermont Auvergne, CNRS, Institut de Chimie de Clermont-Ferrand, Clermont-Ferrand, F-63000, France

[h] Department of Chemistry, Tulane University, New Orleans, Louisiana 70118, United States of America

[*]Corresponding authors: shalu1@uniba.sk (SA); naguib@tulane.edu (MN); olivier.monfort@uniba.sk (OM)

Supplementary Information

Text S1

In dosage variation experiments (Figure S4), an increased trend was observed in the apparent kinetic constant values with increasing dosage of $TiNbO_x$. The constant was 0.0266 min^{-1} for 0.2 g L^{-1} which was 1.5 and 1.3 times the rate constants of 0.04 g L^{-1} and 0.1 g L^{-1} dosage, while it was equivalent when 0.4 g L^{-1} was used. This trend can be ascribed to an increased number of surface-active sites to activate PMS, the higher dosage could lead to more collision, accumulation, or precipitation of $TiNbO_x$, but also more light dispersion or even screening effect from the catalyst [1]. Since, maximum removal of CAF was observed in 120 minutes, with 0.2 g L^{-1} of $TiNbO_x$, it was taken as the optimal condition for further studies (Figure S4a,b).

The concentration of PMS was varied from 0.2 – 5.0 mM (Figure S4c,d). The apparent kinetic constant of CAF degradation first increased up to 0.047 min^{-1} using 2.0 mM PMS and then become constant (Figure S4c). At high concentrations of PMS, the scavenging role of PMS towards the generated ROS such as $^{\bullet}OH$ and $SO_4^{\bullet-}$ is higher [2].

Initial pH value has also a crucial role in the degradation of the pollutants since it has a very strong effect in managing the catalyst charge surface but also the ionic form of the pollutants. Since CAF is a weak electrolyte with a pKa of 10.4 [3], so only a protonated form of caffeine exists in the investigated pH range (between 3 and 9). The effect of initial pH was monitored on CAF degradation by adjusting pH at 3, 5, 7, and 9 after the addition of 0.5 mM of PMS and employing 0.2 g L^{-1} of $TiNbO_x$. Figure S4e shows that with increasing pH from 3 to 9, the degradation efficiency decreases in the following order 84 %, 81 %, 63 %, and 27 %, respectively, after 2 hours of reaction. Likewise, the apparent kinetic constants decrease with increasing pH from 0.021 min^{-1} to 0.002 min^{-1} (Figure S4f). The pH_{zpc} value of $TiNbO_x$, was determined to be 5.64 by using the drift method (Figure S5) [4], which suggested surface of $TiNbO_x$ will be negatively charged at pH > pH_{zpc} and positively charged at pH < pH_{zpc}. Thereby, in acidic pH, $TiNbO_x$ is positively charged and better interacts with CAF especially ketone and aromatic functions which are rich in electrons, while in alkaline pH electrostatic repulsions might occur. Considering pH variation, we found experiments conducted by utilizing 0.5 mM PMS in deionized water without pH adjustment, resulted in maximum degradation of pollutants.

Text S2

The contribution percentage of reactive oxygen species (ROS) in the degradation of CAF and sulfamethoxazole (SMX) in the presence of different scavengers, such as TBA, ISOP, and ISOP+FFA, can be calculated by following the equations S1, S2, and S3:

$$[\bullet OH]\% = \frac{k'_{control} - k'_{TBA}}{k'_{control}} \times 100\% \quad \text{(S1)}$$

$$[SO_4^{\bullet -}]\% = \frac{\left(k'_{control} - k'_{ISOP}\right) - \left(k'_{control} - k'_{TBA}\right)}{k'_{control}} = \frac{k'_{TBA} - k'_{ISOP}}{k'_{control}} \times 100\% \quad \text{(S2)}$$

$$[^1O_2]\% = \frac{\left(k'_{control} - k'_{ISOP+FFA}\right) - \left(k'_{control} - k'_{ISOP}\right)}{k'_{control}} = \frac{k'_{ISOP} - k'_{ISOP+FFA}}{k'_{control}} \times 100\% \quad \text{(S3)}$$

Text S3

X-ray photoelectron spectroscopy (XPS) is a well-known advanced sensitive technique for the detection of chemical changes in the proximity of atoms forming the surface in the depth from 1 to 10 nm. Thereby, high-resolution spectra of Ti 2p, Nb 3d, O 1s, and C 1s present in $TiNbO_x$ were examined to explore its surface chemistry (Fig. S11). The peak fitting of these spectra is presented in Fig. S12. The Ti 2p spectra of the $TiNbO_x$ sample consist of doublet Ti $2p_{3/2}$ and Ti $2p_{1/2}$ lines at positions 458.90 eV and 464.6 eV, respectively (Fig. S12a-c). Notably, the area of $2p_{3/2}$ and Ti $2p_{1/2}$ correspond to the theoretical ratio 2:1. The Ti 2p spectra represent the presence of Ti^{4+} ions in the TiO_2 oxide and the $Ti_2Nb_{10}O_{29}$ consistently with the results of XRD analysis [5]. The Nb 3d spectra (Fig. S12d-f) consist of Nb $3d_{5/2}$ and Nb $3d_{3/2}$ lines at positions 207.3 eV and 210.0 eV, respectively. The corresponding peak area meets the theoretical ratio of 3:2. The splitting of doublet lines in the Nb 3d spectra corresponds to the Nb^{5+} ions in the structure of $Ti_2Nb_{10}O_{29}$

[6]. The O 1s spectra (Fig. S12g-i) were fitted by component at 530.2 eV corresponding to metal oxide bonds (Ti-O, Nb-O), at 531.4 eV to hydroxyl groups bonded to metallic elements and defective oxygen sites, and at 532.6 eV to oxygen-containing organic contaminants and adsorbed water. The C 1s spectra (Fig. S12j-l) of the consist of C-C (C-H), C-O, C=O, and O-C=O components at positions 248.8 eV, 286.3 eV, 287.8 eV, and 288.8 eV. These components are assigned to adventitious carbon contaminants arising due to the usage of MXene as template material (Figure S11d) [7] and exposure of samples to ambient air.

Text S4

To estimate the role of the main reactive oxygen species (ROS) (equation S4), second-order rate constants were considered between selected ROS and pollutants (Table S4).

$$\frac{c_{quencher} \times k_{oxidant\ species,\ quencher}}{c_{quencher} \times k_{oxidant\ species,\ quencher} + C_{pollutant} \times k_{oxidant\ species,\ pollutant}} \quad \text{(S4)}$$

where $c_{quencher}$ and $c_{pollutant}$ were the initial concentrations of scavenger and pollutants, while $k_{oxidant\ species,quencher}$ was the second order rate constant for the targeted ROS and $k_{oxidant\ species,pollutant}$ was the rate constant for pollutant and the targeted ROS, respectively.

Table S1 EDS analysis table for MXene ($Ti_{0.75}Nb_{0.25}CT_x$) and $TiNbO_x$ derived from MXene.

Element	$Ti_{0.75}Nb_{0.25}CT_x$	$TiNbO_x$
Ti	18.06±2.83	13.13±0.98
Nb	5.52±0.55	4.19±0.37
O	24.05±0.73	68.65±2.28
C	36.64±2.34	13.02±3.26
F	11.35±0.71	0.15±0.14
Cl	4.04±0.45	0.01±0.01
Al	0.34±0.21	0.86±0.09

Table S2 LC-MS data of SMX degradation by-products.

Compound	Rt *(min)*	Exp *[M+H]*$^+$	Theor *[M+H]*$^+$	Δ_{mmu}	Exp. *[M-H]*$^-$	Theor. *[M-H]*$^-$	Δ_{mmu}	Molecular formula	Proposed Structure
SMX	3.20	254.0588 276.0407 *[M+Na]*$^+$	254.0594	0.57	252.0445	252.0437	0.77	$C_{10}H_{11}N_3O_3S$	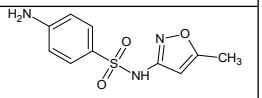
P1	2.28	254.0587	254.0594	0.69	252.0445	252.0437	0.75	$C_{10}H_{11}N_3O_3S$	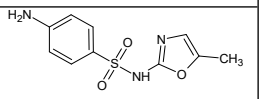
P2	1.92	270.0537	270.0543	0.65	268.0398	268.0387	1.11	$C_{10}H_{11}N_3O_4S$	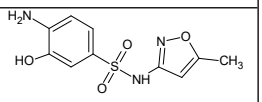
P3	3.24				284.0347	284.0336	1.16	$C_{10}H_{11}N_3O_5S$	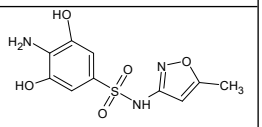
P4	3.16	254.0587	254.0594	0.70	252.0444	252.0437	0.67	$C_{10}H_{11}N_3O_3S$	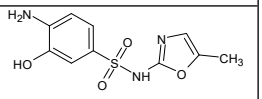
P5	1.92				172.0064	172.0063	0.08	$C_6H_7NO_3S$	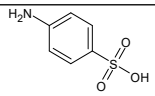
P6	1.13	99.0556	99.0553	0.28				$C_4H_6N_2O$	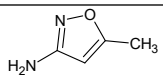
P7	1.29				196.0178	196.0175	0.30	$C_7H_7N_3O_2S$	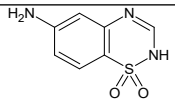

P8	4.21	268.0383	268.0387	0.32	266.0241	266.0230	1.08	$C_{10}H_9N_3O_4S$	
P9	3.17	254.0588	254.0594	0.63	252.0445	252.0437	0.71	$C_{10}H_{11}N_3O_3S$	
P10	2.09	272.0691	272.0700	0.87	270.0553	270.0543	1.10	$C_{10}H_{13}N_3O_4S$	
P11	1.66	288.0641	288.0649	0.78	286.0504	286.0492	1.16	$C_{10}H_{13}N_3O_5S$	

Table S3 Physicochemical characteristics of tertiary effluents of WWTP Bratislava-Petrzalka collected on 10/10/2023 and provided by BVS a.s. (Bratislava Water Company)

Test	Quantity
Chemical oxygen demand	26 mg L^{-1}
Biological oxygen demand	3.0 mg L^{-1}
Non-dissolved matter at 105 °C	10 mg L^{-1}
Total inorganic nitrogen	9.31 mg L^{-1}
Total phosphor	0.55 mg L^{-1}

Pollutants	$k_{\bullet OH}$ **[$M^{-1}s^{-1}$]**	$k_{SO_4^{-\bullet}}$ **[$M^{-1}s^{-1}$]**	$k_{^1O_2}$ **[$M^{-1}s^{-1}$]**	**Reference**

Caffeine	6.40×10^9	2.39×10^9	2.90×10^7	8,9
Sulfamethoxazole	6.98×10^9	2.98×10^9	1.34×10^6	10,11

Table S4 Second order rate constants of pollutants with different reactive oxygen species (ROS).

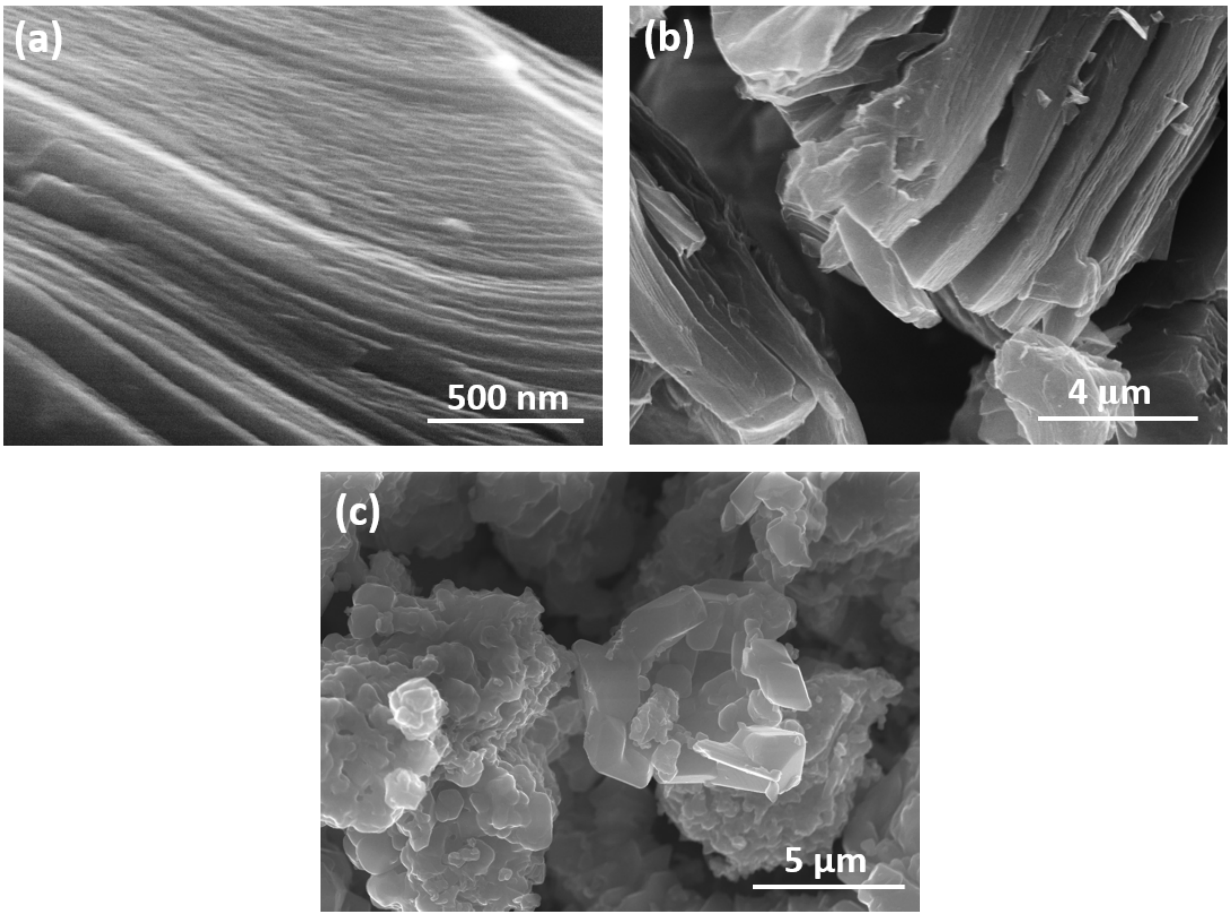

Fig. S1 SEM images of (a) $(Ti_{0.75}Nb_{0.25})_2AlC$, (b) $(Ti_{0.75}Nb_{0.25})_2CT_x$ and its derived (c) $TiNbO_x$.

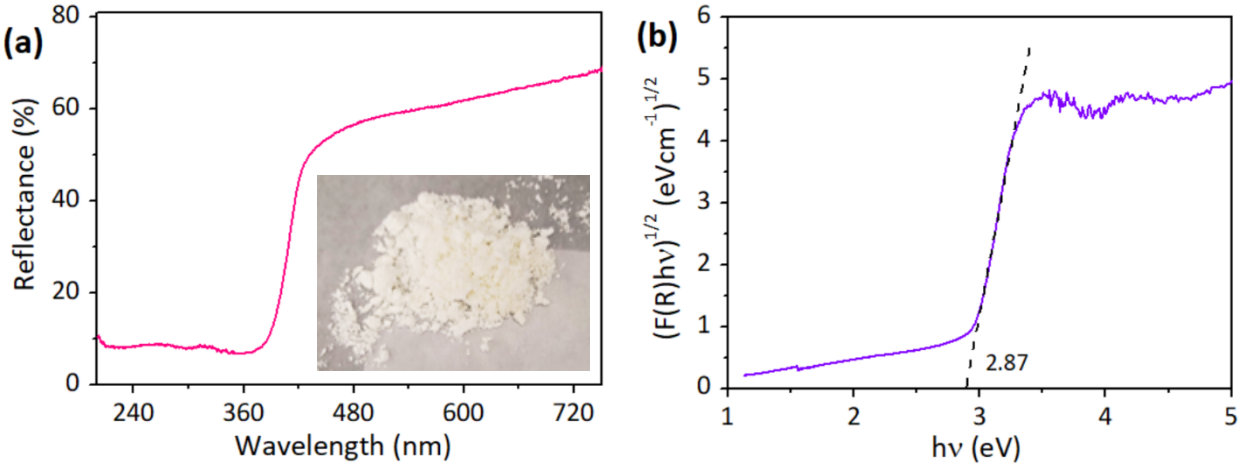
(a)
Reflectance (%)
Wavelength (nm)
0
20
40
60
80
240
360
480
600
720
(b)
(F(R)hν)^1/2 (eVcm^-1)^1/2
hν (eV)
2.87
0
1
2
3
4
5
6
1
2
3
4
5

Fig. S2 (a) DRS spectra of $TiNbO_x$ and their corresponding (b) Tauc's plot. Inset in (a) shows image of $TiNbO_x$ powder.

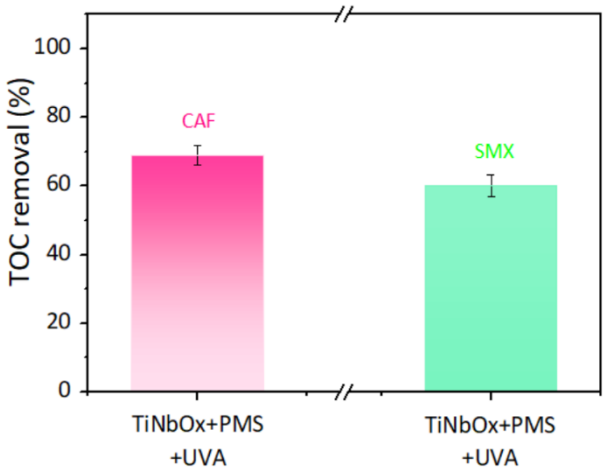

Fig. S3 Evaluation of mineralization extents (TOC removal in %) of CAF and SMX degradation using $TiNbO_x$ under UVA irradiation in the presence of PMS after 2h.

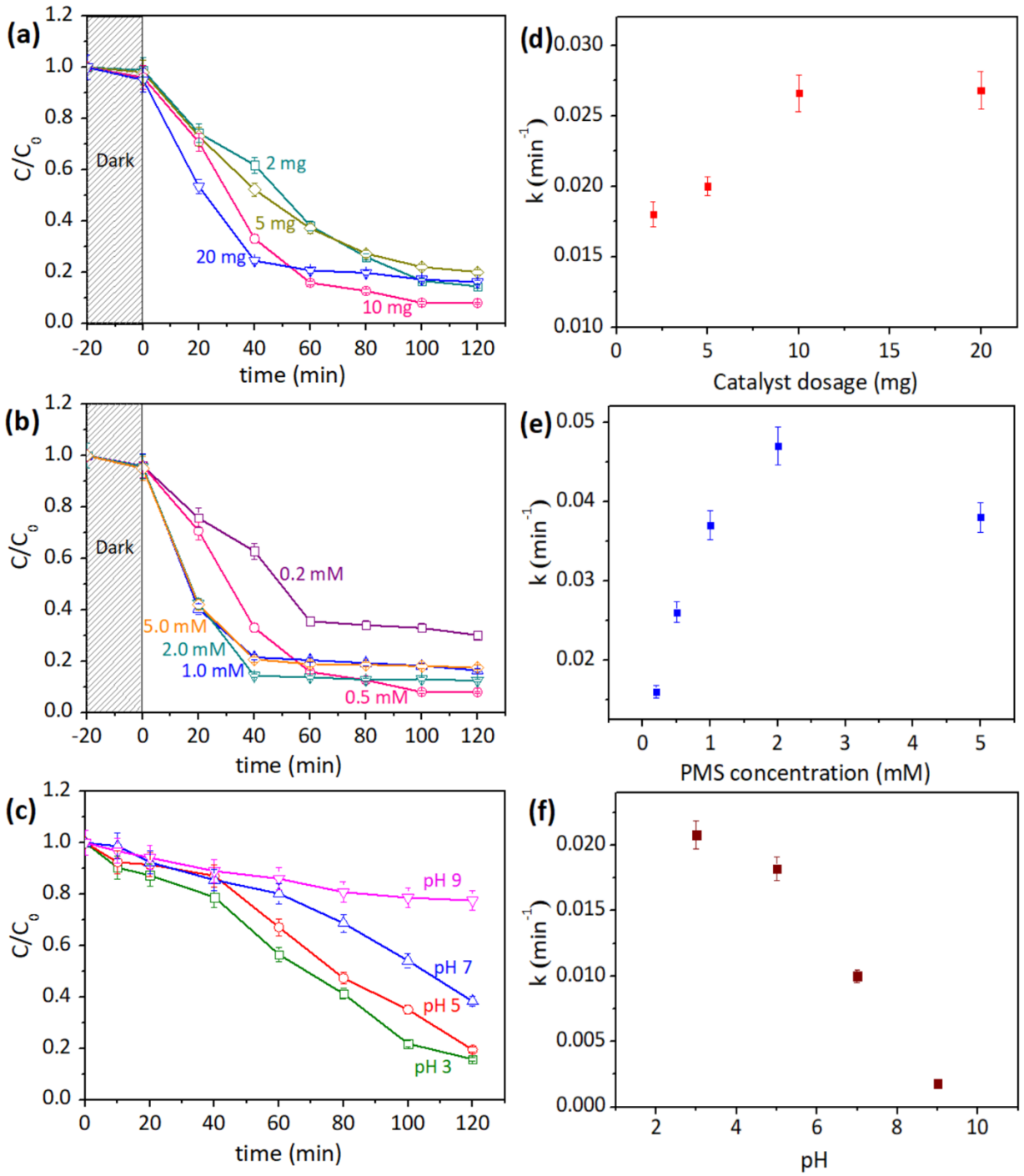
(a)
C/C0
time (min)
Dark
2 mg
5 mg
20 mg
10 mg
(b)
C/C0
time (min)
Dark
0.2 mM
5.0 mM
2.0 mM
1.0 mM
0.5 mM
(c)
C/C0
time (min)
pH 9
pH 7
pH 5
pH 3
(d)
k (min-1)
Catalyst dosage (mg)
(e)
k (min-1)
PMS concentration (mM)
(f)
k (min-1)
pH

Fig. S4 CAF degradation with (a) different $TiNbO_x$ dosages in the presence of 0.5 mM PMS; (b) different PMS concentrations using 0.2 g L^{-1} $TiNbO_x$ and (c) different pH using 0.2 g L^{-1} $TiNbO_x$ in the presence of 0.5 mM PMS. Initial concentration of CAF was 50 μM at natural pH of deionized (DI) water and (d-f) corresponding rate constant dependences on the pH values.

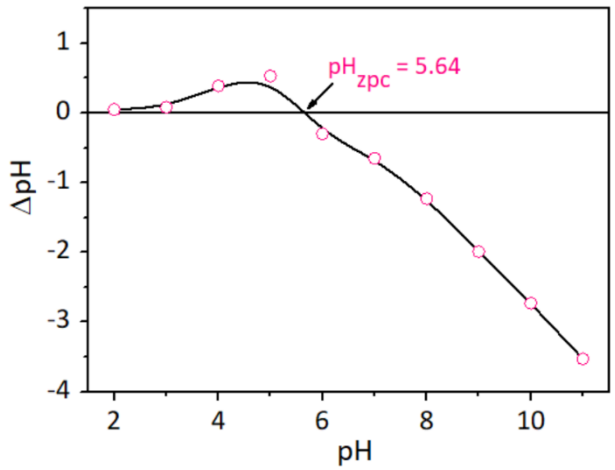

Fig. S5 Assessment of pH of zero-point charge (pH_{PZC}) of $TiNbO_x$ using the drift method.

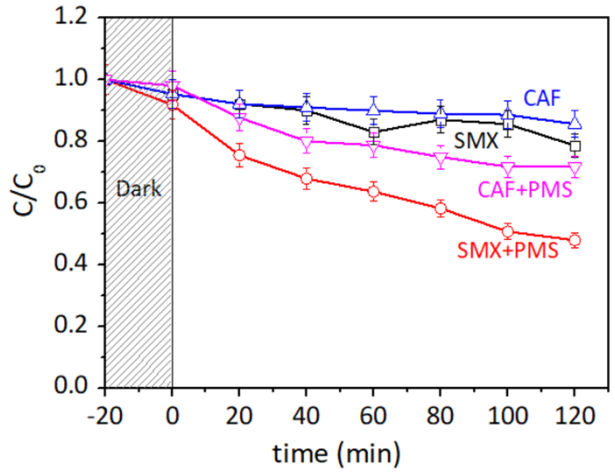

Fig. S6 Degradation curves of CAF and SMX by using 0.2 g L^{-1} of TiO_2 prepared from the thermal oxidation of Ti_2CT_x MXene, with and without 0.5 mM PMS under UVA irradiation at natural pH.

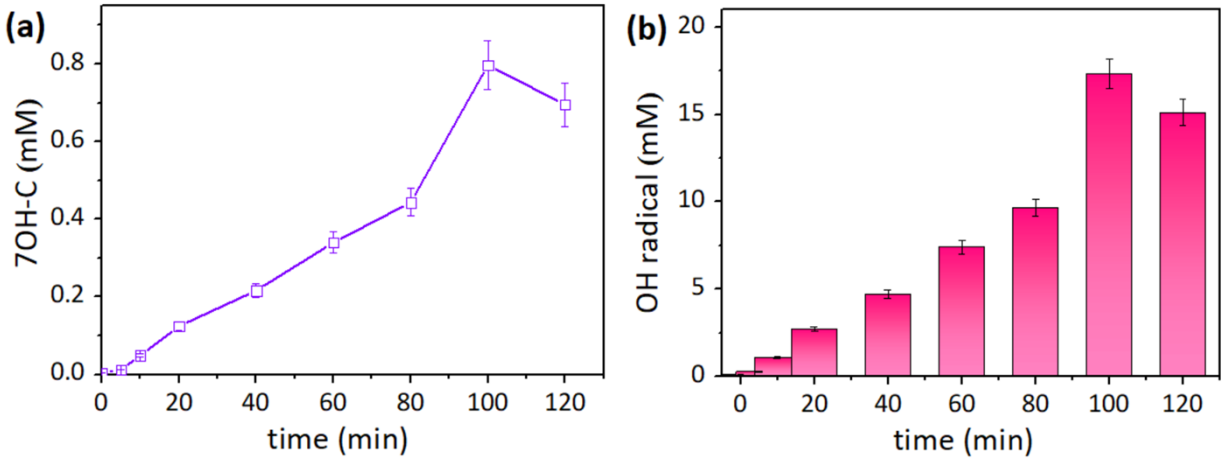
(a)
7OH-C (mM)
0.0
0.2
0.4
0.6
0.8
0
20
40
60
80
100
120
time (min)
(b)
OH radical (mM)
0
5
10
15
20
0
20
40
60
80
100
120
time (min)

Fig. S7 (a) 7-hydroxycoumarin (7OH-C) production using coumarin as probe molecule at natural pH under UVA using 0.2 g L^{-1} $TiNbO_x$ in the presence of 0.5 mM PMS and (b) the corresponding production of hydroxyl radicals calculated from the 4.6% production of 7OH-C [12].

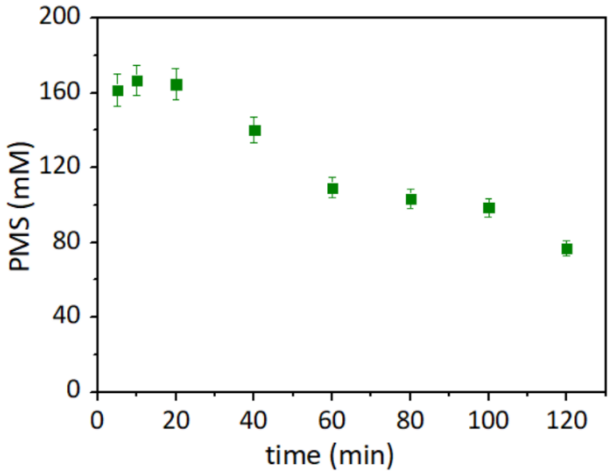

Fig. S8 Spectrophotometric determination of PMS consumption during the degradation of CAF at natural pH under UVA using 0.2 g L^{-1} $TiNbO_x$ in the presence of 0.5 mM PMS.

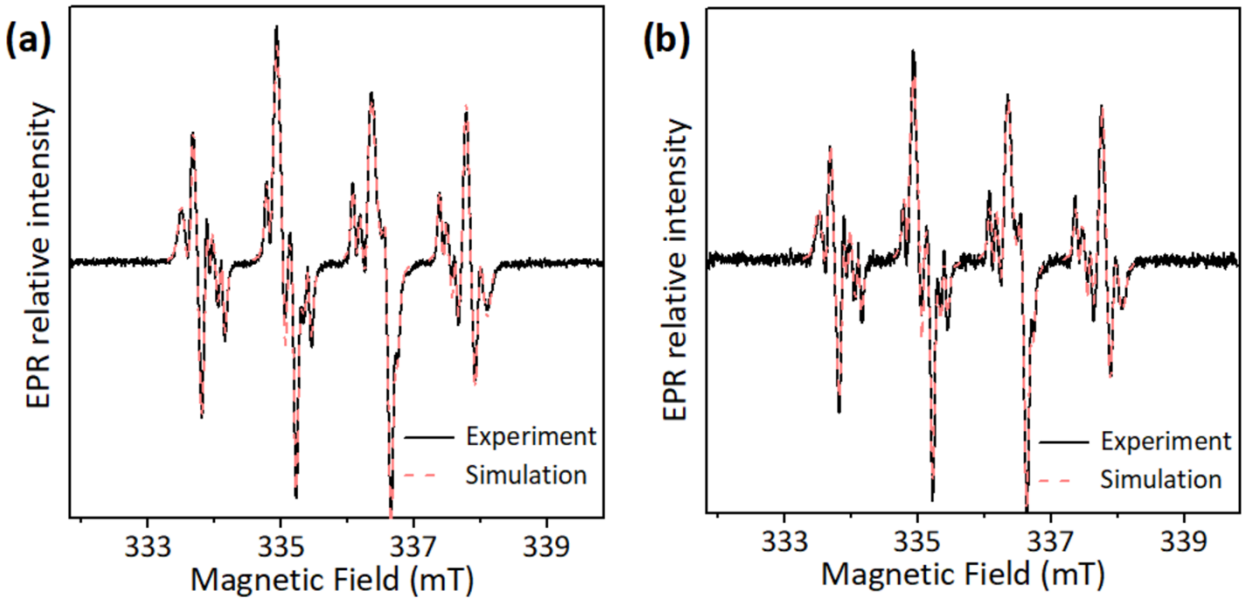

Fig. S9 Experimental and simulated EPR spectra of $TiNbO_x$/CAF/PMS in (a) aerated and (b) deaerated aqueous suspensions measured after UVA exposure (LED@365 nm; radiation dose 6.4 J cm^{-2}) in the presence of BMPO spin trap. Initial concentrations: $c(TiNbO_x)$ = 0.2 g L^{-1}, c_0(CAF) = 50 μM, c_0(PMS) = 0.5 mM, c_0(BMPO) = 35 mM.

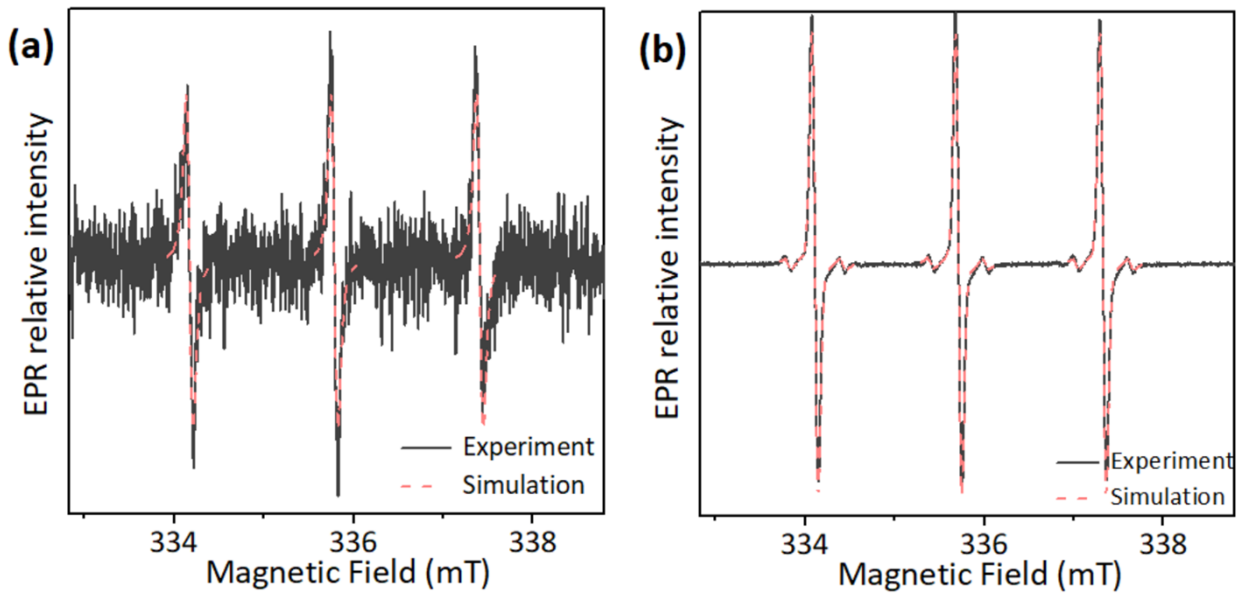
(a)
EPR relative intensity
Experiment
Simulation
334
336
338
Magnetic Field (mT)
(b)
EPR relative intensity
Experiment
Simulation
334
336
338
Magnetic Field (mT)

Supplementary Information

Fig. S10 Experimental and simulated EPR spectra of stable free radical Tempone formed in (a) $TiNbO_x$/SMX/TMPO/air suspension upon UVA exposure (LED@365 nm; radiation dose 6.4 J cm^{-2}) with initial concentrations: $c(TiNbO_x) = 0.2$ g L^{-1}, $c_0(SMX) = 50$ µM, $c_0(TMPO) = 50.0$ mM and (b) PMS/TMPO/air in dark with initial concentrations $c_0(PMS) = 0.24$ mM, $c_0(TMPO) = 0.24$ mM. Spin Hamiltonian parameters for stable nitroxide free radical with resolved ^{13}C satellites obtained from simulation analysis: $a_N = 1.612$ mT, a_{13C} (2 x ^{13}C) = 0.245 mT, a_{13C} (6 x ^{13}C) = 0.639 mT; $g = 2.0057$

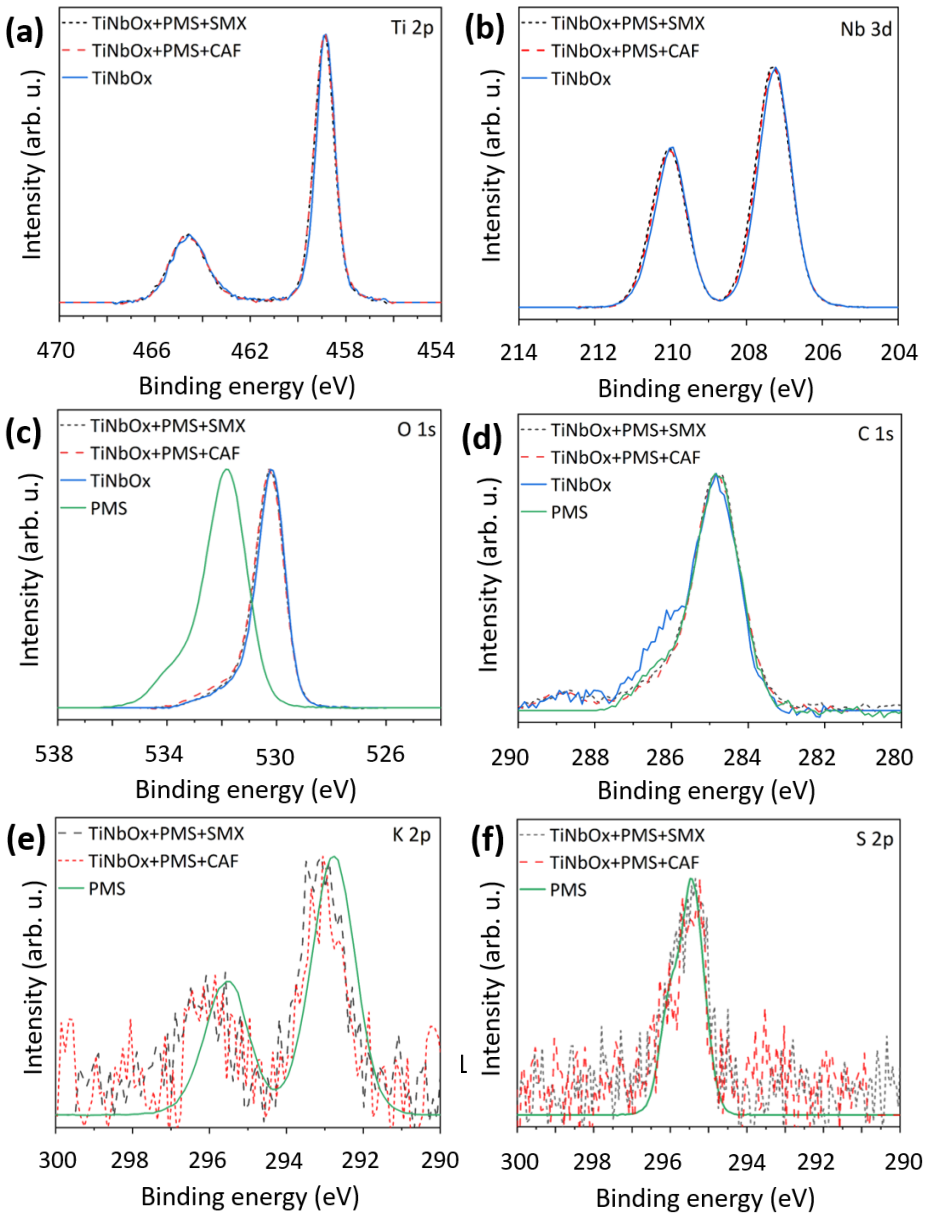

Fig. S11 High-resolution spectra of Ti 2p (a), Nb 3d (b), O 1s (c), C 1s (d), K 2p (e), and S 2p (f) of $TiNbO_x$ sample before and after CAF or SMX degradation. The spectra are referenced using peak at 284.8 eV corresponding to C-C/C-H bonds.

Supplementary Information

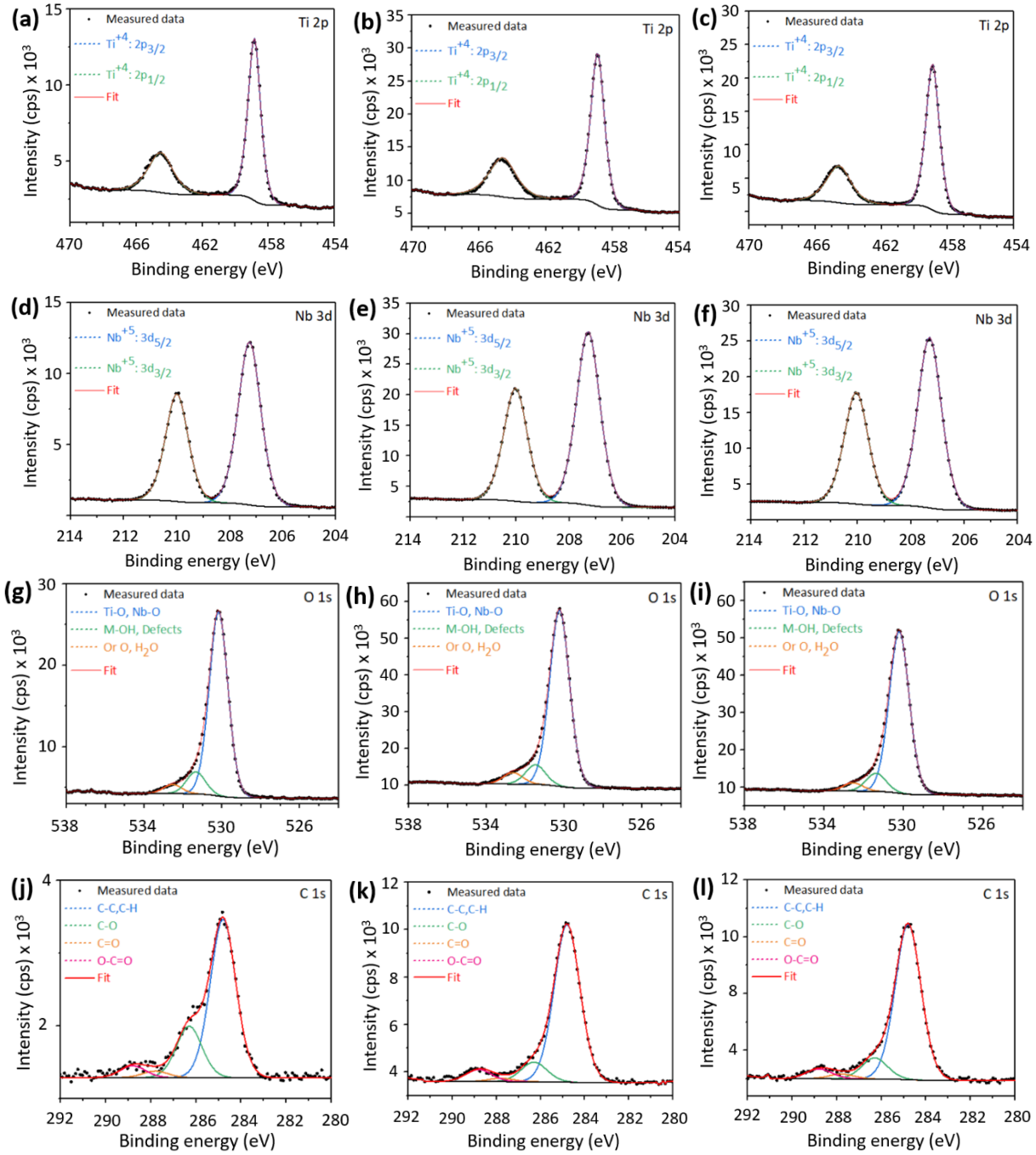

Fig. S12 Peak fitting of high resolution XPS spectra of Ti 2p, Nb 3d, O 1s, C 1s for $TiNbO_x$ sample (a,d,g,j) before and after (b,e,h,k) CAF and (c,f,i,l) SMX degradation. The spectra are referenced using peak at 284.8 eV corresponding to C-C/C-H bonds.

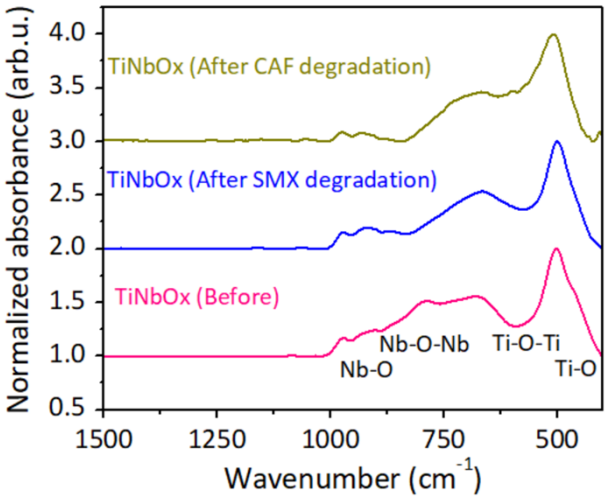

Fig. S13 FTIR spectra of $TiNbO_x$ before and after SMX and CAF degradation.

References

[1] Beheshti, F., Tehrani, R.M.A., Khadir, A. Sulfamethoxazole removal by photocatalytic degradation utilizing TiO_2 and WO_3 nanoparticles as catalysts: analysis of various operational parameters. *Inter. J. Environ. Sci. Technol.* **2019**, *16*, 7987-7996.

[2] U. Ushani, X. Lu, J. Wang, Z. Zhang, J. Dai, Y. Tan, S. Wang, W. Li, C. Niu, T. Cai, N. Wang and G. Zhen, Sulfate radicals-based advanced oxidation technology in various environmental remediation: A state-of-the–art review. *Chem. Eng. J.* 2020, **402**, 126232.

[3] J.A. Quintero-Jaramillo, J.I. Carrero-Mantilla and N.R. Sanabria-Gonzalez, A review of caffeine adsorption studies onto various types of adsorbents. *Sci. World J.* 2021, **2021**, 1-18.

[4] M. Khanal, D. Rai, R. Khanal and A. Bhattarai, Determination of point zero charge (PZC) of homemade charcoals of shorea robusta (Sakhuwa) and pinus roxburghii (Salla). *Inter. J. Eng. Res. Technol.* 2020, **9(10)**, 2278-0181.

[5] M.C. Biesinger, L.W. Lau, A.R. Gerson and R.S.C. Smart, Resolving surface chemical states in XPS analysis of first row transition metals, oxides and hydroxides: Sc, Ti, V, Cu and Zn. *Appl. Surf. Sci.* 2010, **257(3)**, 887-898.

[6] J.J.R. Rumble, D.M. Bickham and C.J. Powell, The NIST X-ray photoelectron spectroscopy database. *Surf. Interface Anal.* 1992, **19(1-12)**, 241-246.

[7] M.C. Biesinger, Accessing the robustness of adventitious carbon for charge referencing (correction) purposes in XPS analysis: Insights from a multi-user facility data review. *Appl. Surf. Sci.* 2022, **597**, 153681.

[8] T.P. Devasagayam, J.P. Kamat, H. Mohan and P.C. Kesavan, Caffeine as an antioxidant: inhibition of lipid peroxidation induced by reactive oxygen species. *Biochim. Biophys. Acta* 1996, **1282**, 63-70.

[9] M. Nihemaiti, D.B. Miklos, U. Hübner, K.G. Linden, J.E. Drewes and J.-P. Croue, Removal of trace organic chemicals in wastewater effluent by UV/H_2O_2 and UV/PDS. *Water Res.* 2018, **145**, 487-497.

[10] L. Gao, Q. Mao, S. Luo, L. Cao, X. Xie, Y. Yang, Y. Deng and Z. Wei, Experimental and theoretical insights into kinetics and mechanisms of hydroxyl and sulfate radicals-mediated degradation of sulfamethoxazole: Similarities and differences. *Environ. Pollut.* 2020, **259**, 113795.

[11] A.M. Lastre-Acosta, B.S. Cristofoli, M.P.S. Parizi, D.C.A.O. Nascimento, A.C.S.C. Teixeira, Photochemical persistence of sulfa drugs in aqueous medium: kinetic study and mathematical simulations. *Environ. Sci. Pollut. Res.* 2021, **28**, 23887-23895.

[12] A. Marion, M. Brigante and G. Mailhot, A new source of ammonia and carboxylic acids in cloud water: The first evidence of photochemical process involving an iron-amino acid complex. *Atmos. Environ.* 2018, **195**, 179-186.